DESIGN OF TUNABLE/RECONFIGURABLE AND COMPACT MICROWAVE DEVICES

Mi Zhou

Thesis Prepared for the Degree of

MASTER OF SCIENCE

UNIVERSITY OF NORTH TEXAS

May 2014

APPROVED:

Hualiang Zhang, Major Professor
Kamesh Namuduri, Committee Member
Shengli Fu, Committee Member and Chair of the Department of Electrical Engineering
Costas Tsatsoulis, Dean of the College of Engineering
Mark Wardell, Dean of the Toulouse Graduate School

Zhou, Mi. Design of Tunable/Reconfigurable and Compact Microwave Devices. Master of Science (Electrical Engineering), May 2014, 53 pp., 3 tables, 32 illustrations, references, 48 titles.

With the rapid development of the modern technology, radio frequency and microwave systems are playing more and more important roles. Since the time the first microwave device was invented, they have been leading not only the military but also our daily life to a new era. In order to make the devices have more practical applications, more and more strict requirements have been imposed. For example, good adaptability, reduced cost and shrank size are highly required. In this thesis, three devices are designed based on this requirement.

At first, a symmetric four-port microwave varactor based 90-degree directional coupler with tunable coupling ratios and reconfigurable responses is presented. The proposed coupler is designed based on the modified structure of a crossover, where varactors are loaded.

Then, a novel reconfigurable 3-dB directional coupler is presented. Varactors and inductors are loaded to the device to realize the reconfigurable performance. By adjusting the voltage applied to the varactors, the proposed coupler can be reconfigured from a branch-line coupler (90-degree coupler) to a rat-race coupler (180 degree coupler) and vice versa.

At last, two types (Type-I and Type-II) of microwave baluns with generalized structures are presented. Different from the conventional transmission-line-based baluns where λ/2 transmission lines or λ/4 coupled lines are used, the proposed baluns are constructed by transmission lines with arbitrary electrical lengths.

ACKNOWLEDGEMENTS

I would like to express my sincere thanks to my major professor Dr. Hualiang Zhang, for providing me the chance to do the research. He has the attitude and the substance of a genius. I have learnt a lot from him. Both my knowledge and skill of doing research have been improved since I met him. I believe that the skill of finding joy of job, which is what I have learnt from him, will always be useful in the future.

I would also like to thank my thesis committee members, Professors Shengli Fu and Kamesh Namuduri for their help.

Next, I want to thank all of my lab mates for their passion, discussion and cooperation.

Finally, I want to thank all my family members for their generous support. They inspired me a lot during my research.

TABLE OF CONTENTS

Page

LIST OF TABLES

Page

LIST OF FIGURES

Page

CHAPTER 1

INTRODUCTION

1.1 Background

With the rapid development of the modern technology, radio frequency and microwave systems are playing more and more important roles. Since the time the first microwave device was invented, they have been leading not only the military but also our daily life to a new era. For the communication systems (e.g. cellphone and base stations), the informations are transmitted and received at radio frequency. For defense systems, microwave devices are applied in radars, satellites and unmanned vehicles. Radio frequency and microwave engineering normally concentrate on the AC signals range from 100 MHz to 1000 GHz. This range includes VHF (very high frequency (30-300 MHz)), UHF (ultra high frequency (300-3000 MHz)), and microwave (3-300 GHz). At the time that the low frequency dominates the field of electrical engineering, standard circuit theory can be used to study the electrical systems. However, as the frequency rises, the wavelength of the signal reduces. Therefore, the phase change of the signals when they travel along the circuits is not neglectable. Under this condition, the standard circuit theory cannot be applied to most of the microwave devices anymore. Instead of that, Maxwell's equations are used to analyze and solve the microwave problems. Also, microwave engineering has become one independent and important branch of the electrical engineering from that time.

1.2 Motivation

More and more strict requirements have been imposed for the microwave devices and components with the advancement of the technology. To meet these requirements, a lot of scientists and engineers have made their efforts on improving the design of RF (radio frequency) and microwave devices. The drawbacks of the previous devices have limited the performance of the whole systems.

Typically there are two main disadvantages. The first one is the large size. For microwave device, especially for those whose working frequencies are less than 1GHz, large size makes the integration difficult. The second disadvantage is the poor adaptability to different systems. In the past, most of the microwave devices are designed to have only one function. For instance, the power dividing ratios of the couplers are mostly fixed. That means a 3 dB coupler can only be applied to the systems which need an equal power splitting ratio. As a result, engineers have to design different devices to fit different systems. A lot of time and money are wasted in this situation.

Addressing these problems becomes the most important task for designing the modern microwave systems. If the size of the devices is reduced, the whole system can be much more compact. Furthermore, if it is possible to make the designed microwave devices applicable to different systems with different characteristics, the procedure of design will be much simpler, and therefore, the cost of the whole system will be much lower.

1.3 Contribution of the Thesis

As discussed in the previous sections, there are several limitations of designing a microwave device. In this thesis, several new tunable and compact microwave devices are presented. 1) A 90 degree branch-line coupler with a wide tuning range of power splitting ratios and reconfigurable responses (can be reconfigured to a crossover) is introduced with the theoretical analysis and the design equations. 2) A novel reconfigurable coupler (can be reconfigured between a branch-line coupler and a rat-race coupler) is presented. 3). The balun featuring generalized structures are introduced.

1.4 Overview of the Thesis

In this thesis, three microwave devices are presented. The idea of designing tunable devices and compact microwave components is intensively studied in this thesis.

In chapter 2, a symmetric four-port microwave varactor based 90-degree directional coupler with tunable coupling ratios and reconfigurable responses is presented. The proposed coupler is designed based on the modified structure of a crossover, where varactors are loaded. By applying suitable biasing voltages to the varactors, the power dividing ratios between the two output ports (i.e. port 2 and port 3) of the coupler can be easily controlled. Moreover, it is found that the realizable power ratio using the proposed structure is very flexible (it could be extremely large or small). Therefore, under the special case when the coupling ratio is tuned to be 1, the proposed coupler is reconfigured to be a crossover. Good isolation and return loss performance have been maintained for different power dividing ratios. To theoretically analyze the proposed device, closed-form design equations are derived using the even-odd mode method. Based on these analytical equations, an experimental prototype working at 1

GHz is designed, fabricated and characterized. The measurement results match well with the simulation and theoretical results, validating the proposed design theory.

In Chapter 3, a novel reconfigurable 3-dB directional coupler is presented. Varactors and inductors are loaded to the device to realize the reconfigurable performance. By adjusting the voltage applied to the varactors, the proposed coupler can be reconfigured from a branch-line coupler (90-degree coupler) to a rat-race coupler (180 degree coupler) and vice versa. During the tuning, good isolation and matching (small reflections) are obtained. To facilitate the design, rigorous theoretical analysis is carried out. Based on the analysis, general design equations are derived. Furthermore, a prototype working at 1 GHz is simulated to prove the design theory. Good agreement is achieved between the simulation and theoretical results.

In Chapter 4, two types (Type-I and Type-II) of microwave baluns with generalized structures are presented. Different from the conventional transmission-line-based baluns where λ/2 transmission lines or λ/4 coupled lines are used, the proposed baluns are constructed by transmission lines with arbitrary electrical lengths. Both of the two types of baluns are designed based on a symmetric four-port structure with one of the ports open-ended. Even-odd mode method is applied to analyze the performance of these baluns. Specifically, for the Type-I design, a symmetrical impedance transformer is employed to realize the desired balun function. For the Type-II design, an asymmetric impedance transforming network is applied. Analytical design equations have been derived for both designs. Based on these equations, two different baluns (Type-I and Type-II) have been designed and simulated. Both of them have very low reflection coefficients at the input port (Port 1) and 3dB insertion losses with a 180 degree phase

difference at the output ports (Port 2 and Port 3). Furthermore, one of the designed prototypes is fabricated and tested. The measurement results match well with the simulation results, which practically prove the design theory.

At last, the conclusions are drawn in Chapter 5. In addition, the direction for future works is presented.

CHAPTER 2

A VARACTOR BASED 90-DEGREE DIRECTIONAL COUPLER WITH TUNABLE COUPLING RATIOS AND RECONFIGURABLE RESPONSES

2.1 Introduction

A coupler is one of the most frequently used RF (radio frequency) devices, which can transfer the power going into its input port to the output ports by splitting it with certain pre-designed ratio [1]. The most popular couplers used are 3 dB couplers, which provide an equal-split power ratio at the output ports [2]-[6]. The unequal-split power couplers are also required frequently in real applications. Meanwhile, a crossover is a kind of four-port RF devices that allows the circuits to avoid using a non-planar structure at the point that needs two wires across each other [7], which meets the requirement of planar integrated circuits. In modern communication systems, couplers and crossovers are widely used.

Typical applications of them include base stations, radar systems, and satellites. In recent years, many people have made efforts on coupler and crossover design [7, 8]. With the advancement of the technology, people are facing more and more design challenges, such as small size, reduced cost, and good adaptability to different systems. In the past, most of the researches concentrate on the dual-band performance [8]-[12] or bandwidth enhancement [13]-[16] of the coupler or crossover, as well as the operating frequency tuning [17]-[21] and shape changing [22] of them. In [4], the authors have designed an integrated coupler (CMOS based) with electronically tuned coupling coefficient. The varactor based tunable coupler was originally designed in [14]. Up to

now, several couplers with tunable power dividing ratios have been presented in the literature [6, 23]. To further enhance the performance of tunable couplers, it is meaningful to integrate the crossover function into it.

In this chapter, a novel planar tunable coupler with tunable coupling ratios and reconfigurable responses is designed. The typical characteristics of this device are summarized as follows: 1) it can be reconfigured between a crossover and a coupler; 2) its power dividing ratio can be easily tuned by adjusting the varactors; 3) it possesses a simple symmetrical structure; 4) the tuning of the power dividing ratio is continuous; 5) the phase difference between the output signals at two ports is very close to 90 degree (kept as a constant) when it works as a directional coupler.

2.2 Theoretical Analysis of the Proposed Device

Fig. 2.1 shows the general schematic diagram of the proposed varactor based coupler with tunable coupling ratios. In this figure, PP' and QQ' are two symmetry planes used in even-odd mode analysis [9]. It can be seen that the coupler consists of three types of transmission lines and two varactor diodes (represented by two capacitors as shown in Fig. 2.1). The characteristic impedance of the transmission lines is defined as Z_1, Z_2, and $Z_3/2$, respectively. Their electrical lengths are $2\theta_1$, θ_2, and $2\theta_3$, and the capacitance of the two varactor diodes is defined as $2C$. The design goal is to make the structure work as a tunable coupler with very flexible coupling ratios under realizable varactors' capacitance values.

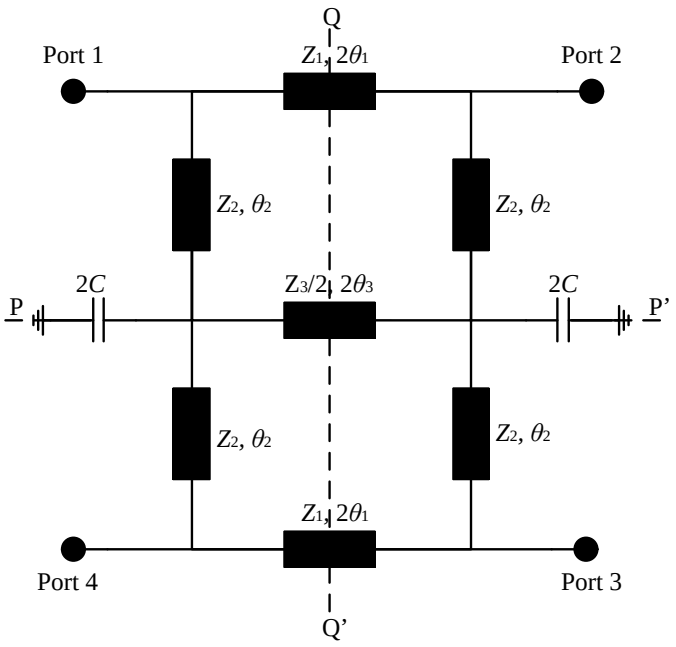

Fig. 2.1 The schematic of the proposed varactor controlled tunable 90-degree directional coupler.

Since the structure in Fig. 2.1 is symmetrical along PP' and QQ' planes, it can be analyzed by even-odd mode method. Fig. 2.2 shows the four sub-circuits (i.e., under even-even, odd-odd, even-odd, and odd-even excitations). Based on these sub-circuits, we can get the input impedances of them. The derived input impedances are listed below:

$$Z_{eo} = \frac{1}{jt_1 / Z_1 + 1/\ jt_2 Z_2} \tag{2-1}$$

$$Z_{oo} = \frac{1}{1/\ jZ_1 t_1 + 1/\ jt_2 Z_2} \tag{2-2}$$

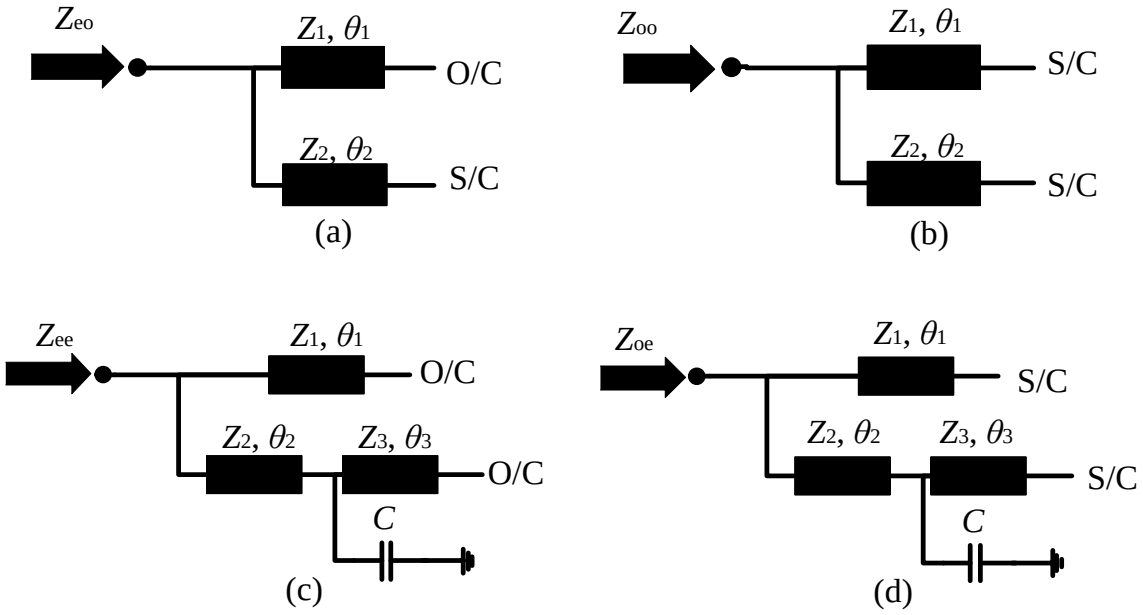

Fig. 2.2. The even-odd mode circuits of the proposed directional coupler under different excitations. (a) Even-odd-mode. (b) Odd-odd-mode. (c) Even-even-mode. (d) Odd-even-mode.

$$Z_{ee} = \frac{1}{\frac{jt_1}{Z_1} + \frac{Z_2 + t_2/(\omega C + t_3/Z_3)}{Z_2/(j\omega C + jt_3/Z_3) + jZ_2^2 t_2}} \tag{2-3}$$

$$Z_{oe} = \frac{1}{\frac{1}{jt_1 Z_1} + \frac{Z_2 + t_2/(\omega C - 1/Z_3 t_3)}{Z_2/(j\omega C + 1/jt_3 Z_3) + jZ_2^2 t_2}} \tag{2-4}$$

where $t_1 = \tan\theta_1$, $t_2 = \tan\theta_2$, $t_3 = \tan\theta_3$, and the designed working frequency is $\omega = 2\pi f$.

From these equations, we can calculate the *S*-parameters of the device by using (2-5) - (2-8) as listed below [9, 10], and [24]:

$$S_{11} = \frac{(\Gamma_{ee} + \Gamma_{oe}) + (\Gamma_{eo} + \Gamma_{oo})}{4} \quad (2\text{-}5)$$

$$S_{21} = \frac{(\Gamma_{ee} - \Gamma_{oe}) + (\Gamma_{eo} - \Gamma_{oo})}{4} \quad (2\text{-}6)$$

$$S_{31} = \frac{(\Gamma_{ee} - \Gamma_{oe}) - (\Gamma_{eo} - \Gamma_{oo})}{4} \quad (2\text{-}7)$$

$$S_{41} = \frac{(\Gamma_{ee} + \Gamma_{oe}) - (\Gamma_{eo} + \Gamma_{oo})}{4} \quad (2\text{-}8)$$

It is found that the *S*-parameters consist of four elements, which are $\Gamma_{ee} + \Gamma_{oe}$, $\Gamma_{ee} - \Gamma_{oe}$, $\Gamma_{oo} + \Gamma_{eo}$, and $\Gamma_{oo} - \Gamma_{eo}$. To further simplify the analysis, we define the following parameters:

$$x = \frac{jt_1}{Z_1} + \frac{Z_2 + t_2/(t_3/Z_3 + \omega C)}{Z_2/(jt_3/Z_3 + j\omega C) + jZ_2^2 t_2} \quad (2\text{-}9)$$

$$y = \frac{1}{jZ_1 t_1} + \frac{Z_2 + t_2/(-1/Z_3 t_3 + \omega C)}{Z_2/(1/jZ_3 t_3 + j\omega C) + jZ_2^2 t_2} \quad (2\text{-}10)$$

$$m = \frac{jt_1}{Z_1} + \frac{1}{jZ_2 t_2} \quad (2\text{-}11)$$

$$n = \frac{1}{jZ_1 t_1} + \frac{1}{jZ_2 t_2} \quad (2\text{-}12)$$

Then the four reflection coefficient (i.e. Γ_{oo} , Γ_{eo}, Γ_{ee}, Γ_{oe}) can be expressed as:

$$\Gamma_{ee} = \frac{1/x - Z_0}{1/x + Z_0} \tag{2-13}$$

$$\Gamma_{eo} = \frac{1/m - Z_0}{1/m + Z_0} \tag{2-14}$$

$$\Gamma_{oo} = \frac{1/n - Z_0}{1/n + Z_0} \tag{2-15}$$

$$\Gamma_{oe} = \frac{1/y - Z_0}{1/y + Z_0} \tag{2-16}$$

Next, based on (2-5) – (2-16), the design equations of the proposed tunable coupler with different performance are derived. First, the equations when it performs as a crossover are derived. In practice, when it is a crossover, the device should have the following properties $S_{11} = S_{21} = S_{41} = 0$, $|S_{31}| = 1$, and $\Gamma_{ee}=\Gamma_{oo}=-\Gamma_{eo}= -\Gamma_{oe}$ [9, 10]. In order to satisfy $\Gamma_{ee} = \Gamma_{oo}$, we should have $x = n$. Similarly, to achieve $\Gamma_{eo} = \Gamma_{oe}$, $m = y$ needs to be satisfied. Also, $\Gamma_{oo}= - \Gamma_{eo}$ needs to be realized. By examining (2-14) and (2-15), the following assumptions have been made to simplify the analysis: $\theta_2 = 90°$, $t_1 = t_3$, and $Z_1 = Z_3$, and $Z_1 = 50\Omega$. Four more equations can be derived by applying those values to (2-9) - (2-12).

After some derivations, we have reached the following design equations when the proposed device performs as a crossover:

$$Z_2^2 = \frac{Z_1^2 t_1}{(1+t_1^2)(t_1 + Z_1 \omega c)} \tag{2-17}$$

$$Z_2^2 = \frac{Z_1^2 t_1^2}{(1+t_1^2)(1 - Z_1 t_1 \omega c)} \tag{2-18}$$

$$Z_1 = Z_0 = 50\Omega \tag{2-19}$$

To satisfy (2-17) and (2-18), θ_1 must be equal to θ_3, which is equal to 45°. The capacitance (C) should be equal to 0 (in practice, a small capacitance value can also guarantee the crossover performance). Finally, for crossover operation, the value of Z_2 is found to be 35 Ω.

Secondly, the design equations for proposed coupler with tunable coupling ratios are derived. In general, we need to find the relationship between the capacitance (C) and the S-parameters. We will show, using the proposed design, the S-parameters can be tuned by adjusting the capacitance (C). By applying the design parameters derived in (2-17) – (2-19), under the coupler mode, we have the following four design equations.

$$\Gamma_{oo} + \Gamma_{eo} = \frac{2Z_1^2 - 2Z_0^2}{Z_1^2 + Z_0^2} = 0 \tag{2-20}$$

$$\Gamma_{oo} - \Gamma_{eo} = \frac{4jZ_0Z_1}{Z_1^2 + Z_0^2} = 2j \tag{2-21}$$

$$\Gamma_{ee} + \Gamma_{oe} = \frac{4jZ_0^2Z_2^2 - 2jZ_0^4}{-Z_0^2\omega^2c^2 + 2jZ_0\omega c + 1} = 0 \tag{2-22}$$

$$\Gamma_{ee} - \Gamma_{oe} = \frac{2jZ_0^2\omega^2c^2 + 2j}{-Z_0^2\omega^2c^2 + 2jZ_0\omega c + 1} \tag{2-23}$$

From (2-20) and (2-22), it is found that $S_{11} = S_{41} = 0$, which means that Port 1 and Port 4 are always highly isolated and matched no matter what value of C is applied (note: this is highly desired). Furthermore, S_{21} and S_{31} are calculated as the summation and subtraction of (2-21) and (2-23), so they are related to the capacitance (C).

Because of this property, it is obvious that the ratio of the output power at Port 2 and Port 3 can be controlled by adjusting the capacitance of the varactors (more details will be presented in the next section).

2.3 Simulation Results

To verify the design theory, the magnitude of the *S*-parameters and the phase difference between S_{21} and S_{31} of an ideal proposed coupler working at 1GHz were calculated. The calculated phase responses are shown in Fig. 2.3, and the calculated magnitude results are shown in Fig. 2.4. In Fig. 2.3, the phase responses of the proposed tunable coupler are obtained by applying (2-6) and (2-7) along with (2-21) and (2-23). Here, the phase difference is plotted versus biasing voltage (*V*) applied to the varactors (the biasing voltage can be translated to capacitance value based on the applied varactors (SMV1265 from Skyworks [25] is used in this project)). It is observed that, no matter what the capacitance is, the phase difference between the two output ports is always 90-degree. Therefore, theoretically, the proposed coupler is a 90-degree coupler (it is worth to point out that the mismatch between the calculated data and the measured data is caused by factors such as the parasitics and losses of the varactors).
In Fig. 2.4, the magnitudes of the *S*-parameters are examined. The figure shows that the S_{31} (blue curve) starts from 1, then it drops while the capacitance increases. For S_{21} (red curve), it starts from 0. When the capacitance increases, the S_{21} curve goes in the opposite direction as S_{31} does. Furthermore, it can be seen that these two curves are almost symmetrical about 0.5 (i.e. the total magnitude of them is always equal to 1). When $|S_{21}|^2$ equals $|S_{31}|^2$ (i.e. at the 3 dB point), the capacitance is about 4.5 pF.

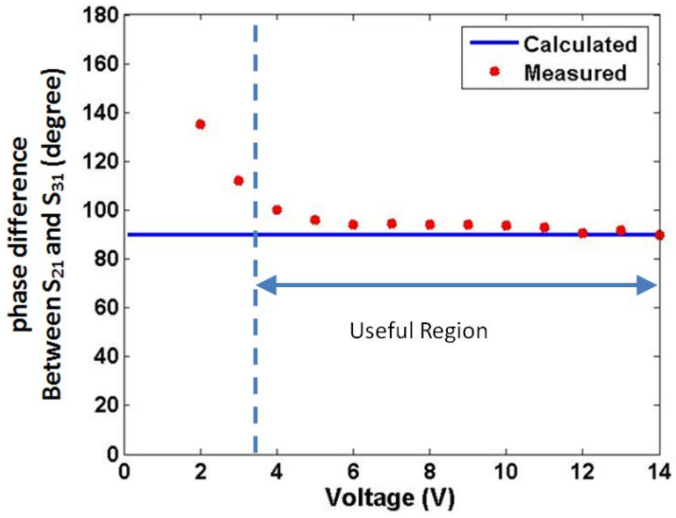

Fig. 2.3. Calculated and measured phase difference between S_{21} and S_{31} versus different control voltage.

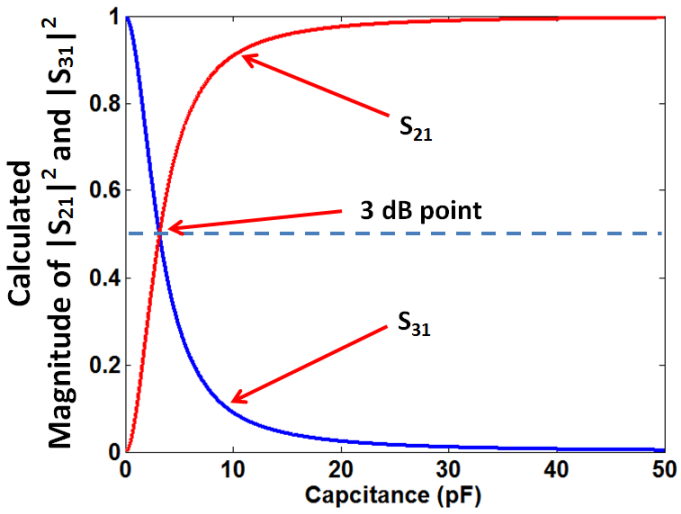

Fig. 2.4. Calculated magnitude of $|S_{21}|^2$ and $|S_{31}|^2$ versus different capacitance.

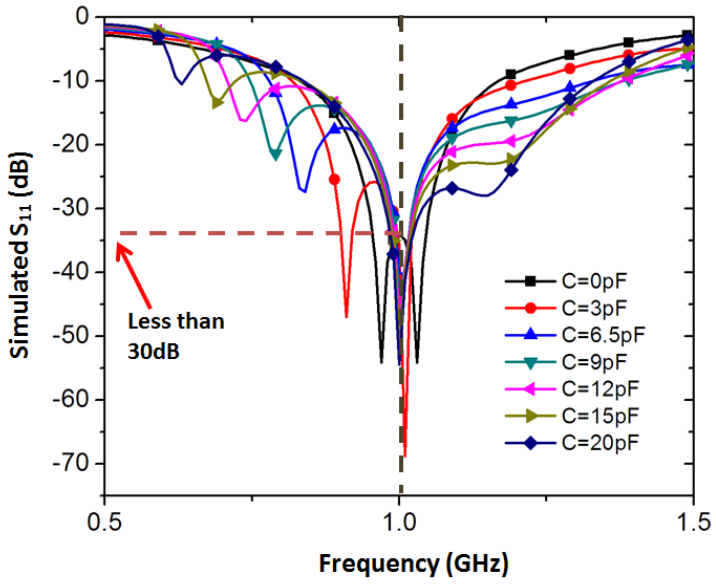

Fig. 2.5. Simulated $|S_{11}|$ when different capacitance is applied.

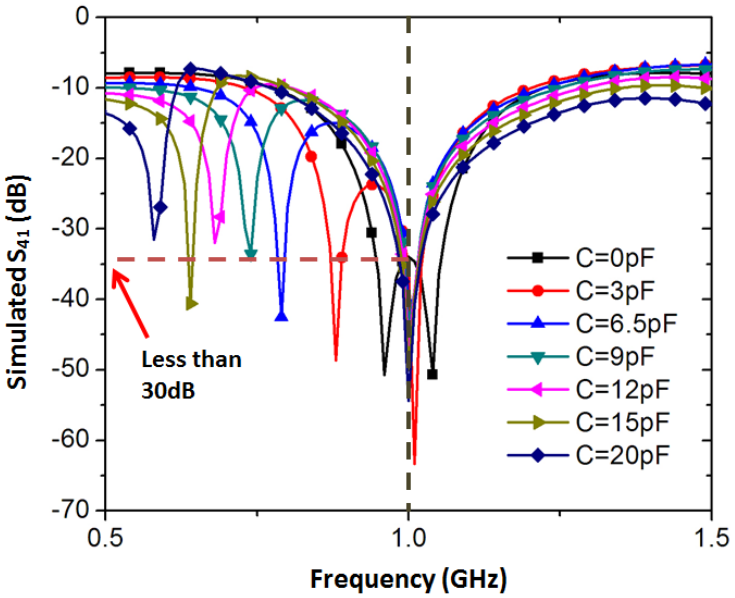

Fig 2.6. Simulated $|S_{41}|$ when different capacitance is applied.

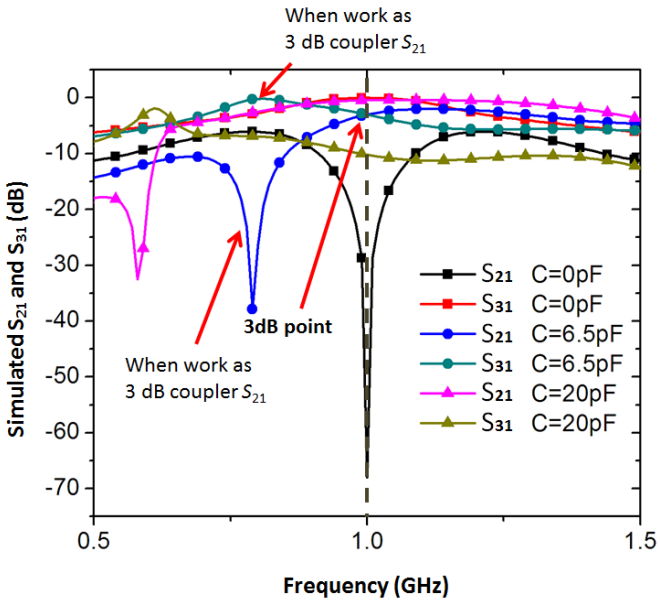

Fig. 2.7. Simulated $|S_{21}|$ and $|S_{31}|$ when different capacitance is applied.

We have also simulated this coupler working at 1GHz using Agilent's Advanced Design System (ADS). The results are given in Figs. 2.5 – 2.7. From these simulation results, the characteristics of this device can be summarized as the following:

- The reflection coefficient ($|S_{11}|$) is below -30 dB at 1 GHz when the capacitance (C) equals 0 pF, and it can be much lower than -60 dB when the capacitance is higher.
- The proposed tunable coupler has a very high isolation ($|S_{41}|$) at the working frequency. The magnitude is greater than 30 dB when C = 0 pF, and greater than 60 dB for other values of the capacitance.
- The power goes out at Port 2 and Port 3 can be controlled by choosing different capacitance. When C is around 0 pF, $|S_{21}|$ is about 70dB. It is an ideal crossover. The power ratio changes continuously by changing C.
- The phase difference between the two output ports (Port 2 and Port 3) is always

90 degree theoretically.

It is clear the simulation results match well with the theoretical results, which further verifies the performance of the proposed tunable directional coupler (the mismatch between the calculated data and the simulated data is due to the loss and interferences of the transmission lines and the capacitors).

2.4 Measured Results

To realize the proposed structure, a prototype has been designed using HyperLynx (previously called IE3D) and fabricated. The photo of the fabricated sample is shown in Fig. 2.8. The dimensions of the coupler are marked in this figure. It was fabricated on the RT/Duriod 5880 printed circuit board, whose substrate thickness is 0.787 mm and the dielectric constant is 2.2. As marked in the figure, on the two sides of the prototype, two DC/RF block networks are applied between the varactors and the coupler to provide the suitable biasing voltage. The values of both the capacitors and the inductors should be large enough so that the DC voltages that used to drive the varactors will not go into the VNA and the RF signals will not go into the DC power supplies. The inductor finally chosen is R20JX from Coilcraft and the varactor is SMV1265 from Skyworks as mentioned before.

The measurement results of the experimental prototype are given in Figs. 2.9 - 2.11. Figs. 2.9 and 2.10 prove that a low reflection coefficient (always below -20dB) and a good isolation (always greater than 20dB) can be achieved during the tuning when the biasing voltage is varied from 0 – 14V. Fig. 2.10 also shows that this component has a good directivity (e.g. directivity at 14V control voltage is plotted here). Fig.

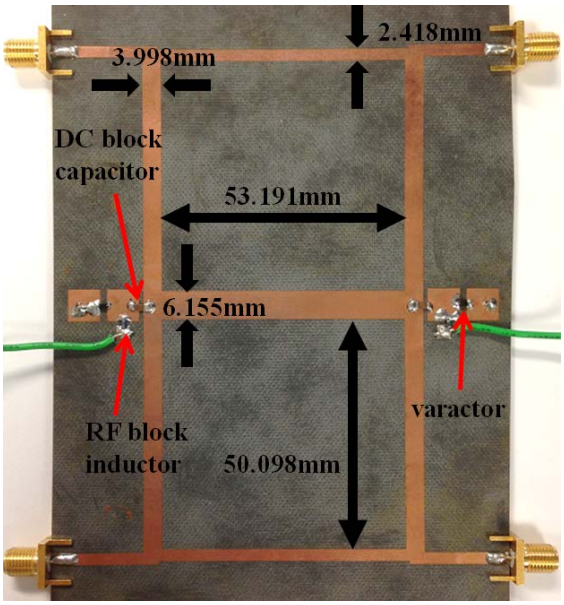

Fig. 2.8. Photo of the fabricated prototype.

2.11 shows the measured magnitudes of S_{21} and S_{31}. When the biasing voltage is 14V, S_{31} is close to 0dB and S_{21} is below -20dB. Under this condition, it performs as a crossover. With the changing of the biasing voltage, the magnitudes of S_{21} and S_{31} change continuously (in opposite directions). At the biasing point of 4.33V, it performs as a 3 dB coupler. When the biasing voltage is below 4.33V, the magnitude of S_{21} becomes larger than that of S_{31}. The measured phase response is given in Fig. 2.12 (for the purpose of easy comparison, we have also plotted the measured phase difference in Fig. 2.3 (red dotted line)). It is found that the phase difference between the two output ports (port 2 and port 3) is smaller than 97 degree when the biasing voltage is larger than 3.8V. This has clearly verified that the fabricated device can be treated as a tunable 90-degree coupler (since this biasing voltage range has covered most of the biasing points when this device performs as a coupler). Overall, the measurement data matches well with the simulation results. For example, the magnitudes of S_{11} and S_{41}

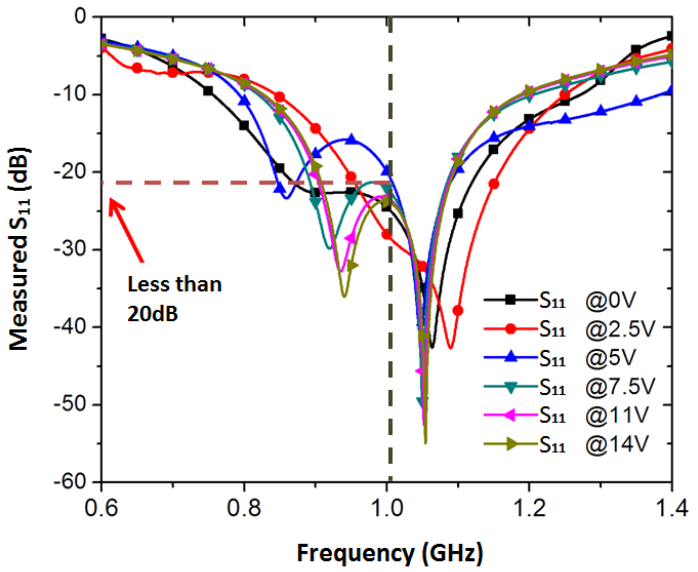

Fig. 2.9. Measured $|S_{11}|$ when different control voltage is applied.

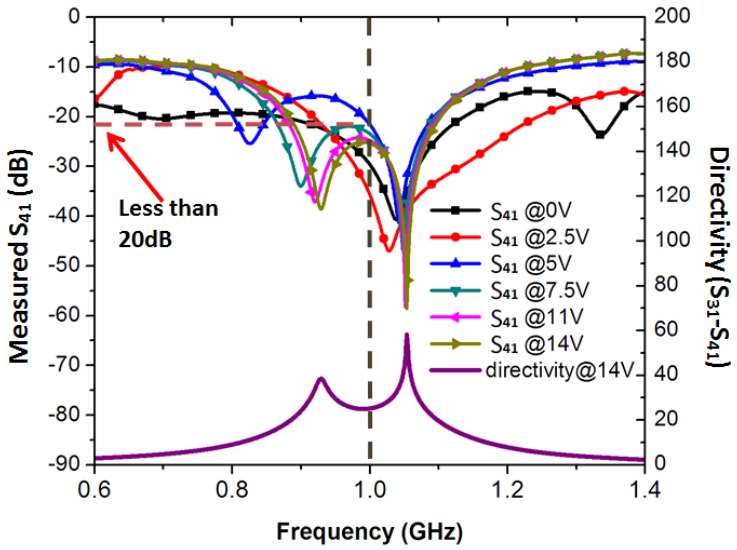

Fig. 2.10. Measured $|S_{41}|$ when different control voltage is applied and measured directivity at 14V.

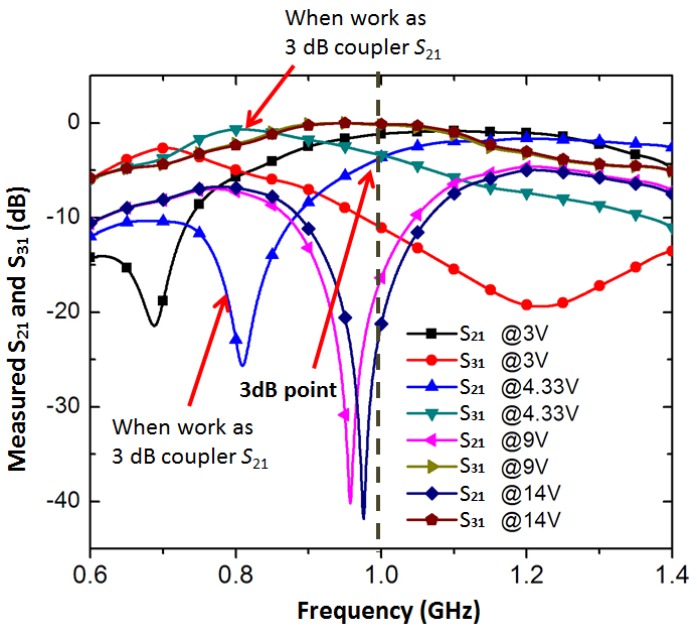

Fig. 2.11. Measured $|S_{21}|$ and $|S_{31}|$ when different control voltage is applied.

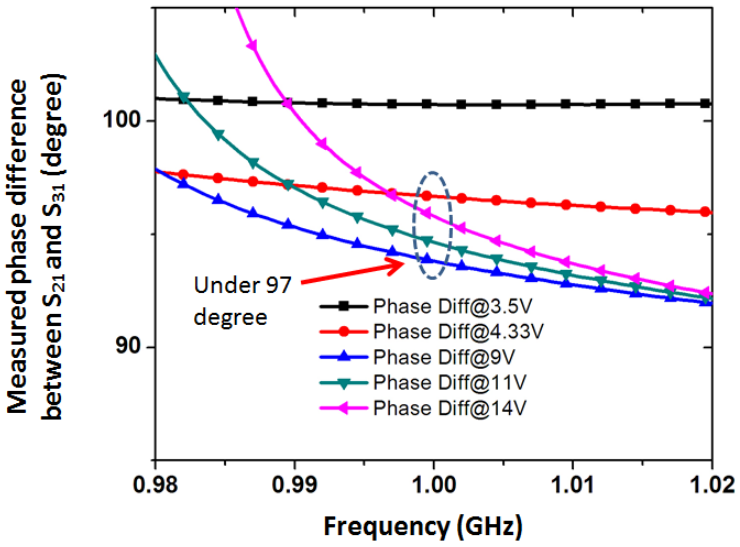

Fig. 2.12. Measured phase difference between S_{21} and S_{31} when different control voltage is applied.

are almost the same as the simulation results. Also, we can see from the perpendicular dashed lines marked in Fig. 2.7 and Fig. 2.11 that, when the coupler works as a 3 dB hybrid, the shapes of the curves are approximately the same (with less than 20 MHz frequency shift caused by the loss of the capacitors and the circuit asymmetry due to the fabrication error).

2.5 Conclusion

The design and implementation of a new varactor based 90-degree coupler with tunable power ratio and reconfigurable response have been presented. Analytical design equations have been derived for the proposed coupler. Based on the design equations, a prototype working at 1 GHz has been designed, fabricated, and characterized. The measurement results match well with the theoretical and numerical results. It is validated that the proposed structure features a large power ratio tuning range and can be reconfigured between a crossover and a coupler. During the tuning, it maintains very good return loss and isolation. Furthermore, since there are only two varactors applied in the proposed structure, it is easy for practical implementations.

CHAPTER 3

A NOVEL 3 DB DIRECTIONAL COUPLER WITH RECONFIGURABLE PERFORMANCE

3.1 Background and Motivation

As said in the last chapter, directional coupler is one of the mostly used power dividing and combining devices in the modern microwave circuits and systems. They can not only be employed in the communication systems such as base stations [26] but also be applied to the defense systems such as satellites and radars to feed the antenna arrays [27]. In addition, they can be applied in the balanced mixers and differential amplifiers [28]. For a branch-line coupler, the phase difference between the output signals is 90 degree, so it is also called a 90 degree coupler. For the rat-race coupler, the phase difference between the output ports is 180 degree or 0 degree.

In the past, most of the couplers only have a fixed phased difference (e.g. 90 degree, 180 degree and 0 degree). However, with the development of the modern technology, a reconfigurable coupler (i.e. a coupler can be reconfigured to realize the couplers with different phase difference) is highly desirable. To address this problem, a lot of researchers and engineers have made their efforts to improve the performance of couplers, but just a few of them have a reconfigurable response.

In the previous section, a 90 degree coupler which can be reconfigured to a crossover is presented. In this section, a novel varactor and inductor-based reconfigurable coupler which can be reconfigured between a branch-line and a rat-race

coupler is presented. To the best of our knowledge, this is for the first time a coupler featuring such a property is designed.

3.2 Design Theory and Simulation Results

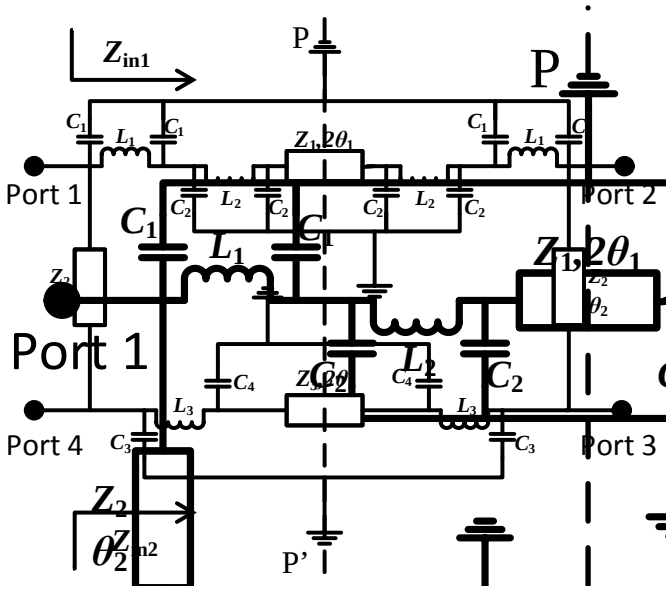

Fig. 3.1. Schematic diagram of the proposed coupler.

Fig. 3.1 shows the general schematic of the proposed reconfigurable coupler. In this figure, C_i (i = 1 - 4) is the capacitance of the varactor, which is the tuning element applied in the coupler. During the tuning / reconfiguration, the varactors labeled with the same number (e.g. C_1, C_2 … as shown in Fig. 3.1) are controlled by the same voltage. Since the coupler features a symmetrical structure, even-odd mode method can be applied to analyze its performance (assuming PP' is the symmetric plane). Z_{in1} and Z_{in2} are the input impedance looking into the branches of the circuit after analyzing along the

symmetric plane. Fig. 3.2 shows its equivalent circuits under the even-mode and odd-mode excitations. Under even-mode excitation, the transmission lines along the symmetric plane (Z_1, Z_3) are open circuited. The odd-mode equivalent circuit is similar to the even-mode equivalent circuit but with the transmission lines along the symmetric plane short circuited (Z_{ein1}, Z_{ein2}, Z_{oin1}, and Z_{oin2} are impedances when Z_{in1} and Z_{in2} are under different modes).

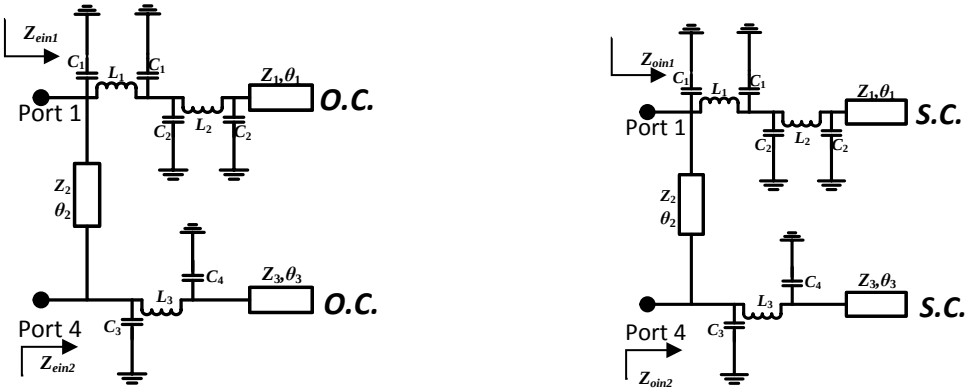

(a) (b)

Fig. 3.2. Equivalent circuit of the proposed coupler under different excitation mode. (a) Under even-mode excitation. (b) Under odd-mode excitation.

Based on the even-mode equivalent circuit, the input impedances (Z_{ein1} and Z_{ein2} as labeled in Fig. 3.2) looking into different branches are given in (3-1) and (3-2).

$$Z_{ein1} = \frac{1}{\frac{1}{\frac{1}{\frac{1}{\frac{1}{j\omega C_2 + j/Z_1 tan\theta_1} + j\omega L_1} + j\omega C_2 + j\omega C_1} + j\omega L_1} + j\omega C_1} \qquad (3-1)$$

$$Z_{ein2} = \frac{1}{\frac{1}{\frac{1}{j\omega C_4 + \frac{jtan\theta_3}{Z_3}} + j\omega L_2} + j\omega C_3} \qquad (3-2)$$

In order to simplify the analysis, the following assumptions are made, $Z_1 = Z_2 = Z_3$ = 70.7Ω, θ_1 = 45°, θ_2 = 90°, and θ_3 = 90°. Substituting these values into (3-1) and (3-2), two new functions are obtained. Following the same procedure, the design equations of the odd-mode equivalent circuit are derived as the following (the same assumptions as the even-mode case are made):

$$Z_{oin1} = \frac{1}{\frac{1}{\frac{1}{\frac{1}{\frac{1}{j\omega C_2 + \frac{1}{jZ_1}} + j\omega L_1} + j\omega C_2 + j\omega C_1} + j\omega L_1} + j\omega C_1} \qquad (3-3)$$

$$Z_{oin2} = \frac{1-\omega^2 C_4 L_2}{j\omega C_4 + j\omega C_3 - j\omega^3 C_3 C_4 L_2} \qquad (3-4)$$

From (3-1)-(3-4) (referring to Fig 3.2), the ABCD matrix of the proposed coupler is [27]:

$$\begin{bmatrix} A & B \\ C & D \end{bmatrix} = \begin{bmatrix} \frac{jZ_2}{Z_{in2}} & jZ_2 \\ \frac{j}{Z_2} + \frac{j}{Z_{in1}Z_{in2}} & \frac{jZ_2}{Z_{in1}} \end{bmatrix} \qquad (3-5)$$

Finally, the *S*-parameters of proposed coupler can be calculated from (3-5). MATLAB is then used to find the solutions for the proper capacitance combinations of the varactors for different coupler performance (i.e. rat-race coupler or branch-line coupler). One set of the possible solutions is listed in Table 3.1 (Note: all of the selected capacitance values can be realized by the commercial varactors).

TABLE 3.1

Values of the Lumped Elements

Element value	**Rat-race coupler**	**Branch-line coupler**
L_1	6 nH	6 nH
L_2	6 nH	6 nH
L_3	8 nH	8 nH
C_1	2.3 pF	1 pF
C_2	5 pF	1.3 pF
C_3	0.2 pF	0.5 pF
C_4	1 pF	1 pF

To verify the design theory, simulation of the proposed structure is conducted by Advanced Design System (ADS) from Agilent. The simulation results are shown in Fig 3.3 and Fig 3.4. Fig 3.3 shows the results of the proposed coupler when it works as a rat-race coupler (i.e. Port 1 or Port 3 is the input port, and Port 2 and Port 4 are the output ports; the parameters given in the second column of Table 3.1 are used for the simulation). Fig 3.4 shows the results of the coupler when it works as a 90-degree

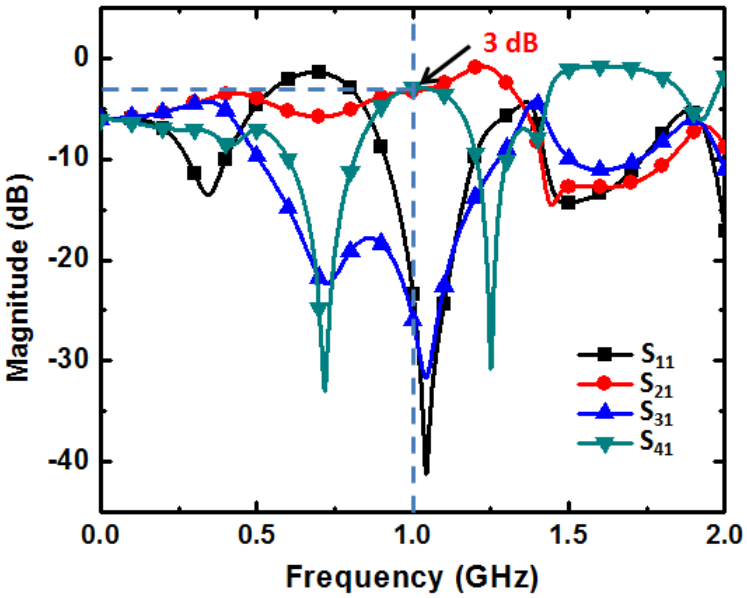
3 dB
0
-10
-20
-30
-40
Magnitude (dB)
0.0
0.5
1.0
1.5
2.0
Frequency (GHz)
S11
S21
S31
S41

(a)

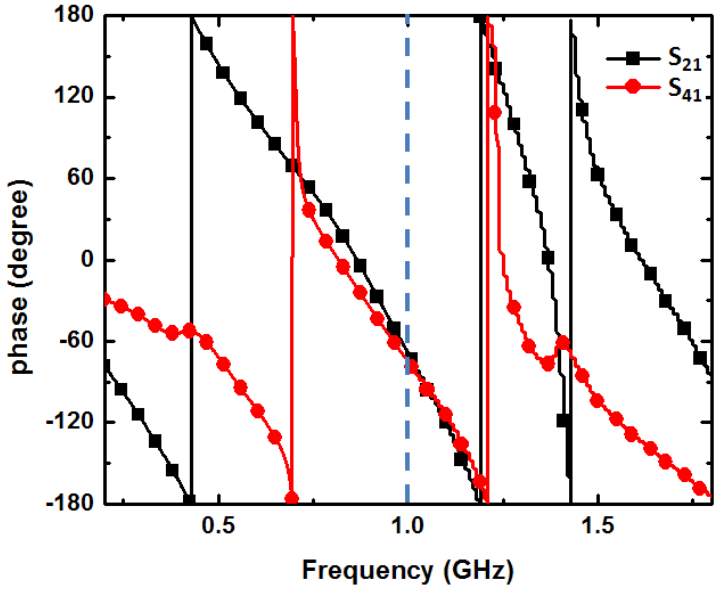
180
120
60
0
-60
-120
-180
phase (degree)
0.5
1.0
1.5
Frequency (GHz)
S21
S41

(b)

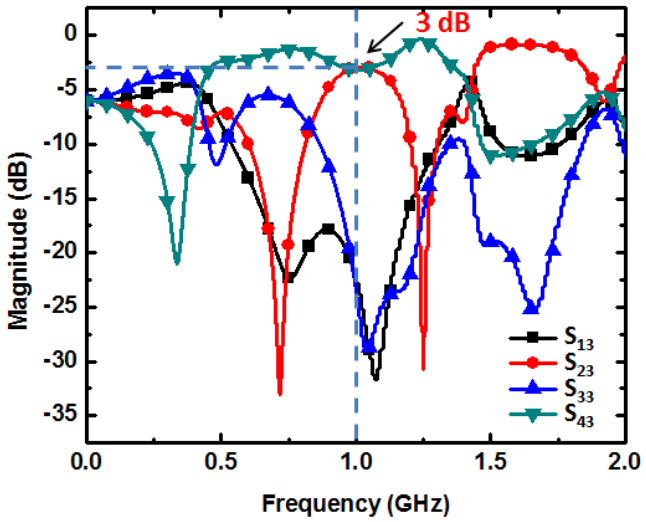

(c)

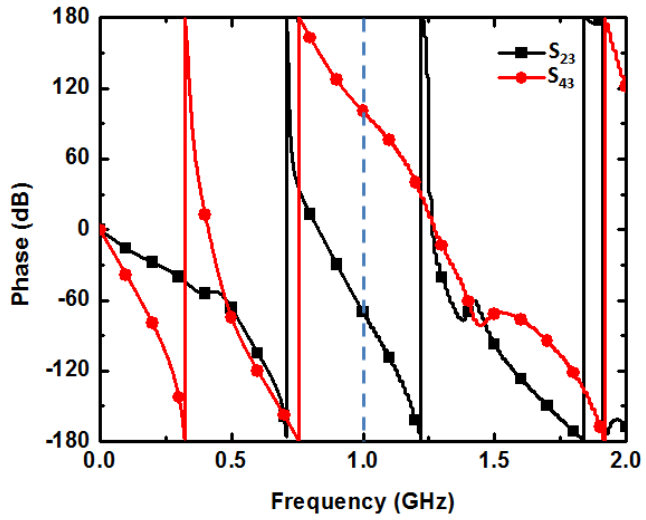

(d)

Fig. 3.3. Simulation results when the proposed coupler works as a rat-race coupler: (a) Magnitude performance when feeding from Σ port. (b) Phase difference between the output ports when feeding from Σ port. (c) Magnitude results when feeding from Δ port. (d) Phase difference between the output ports when feeding from Δ port.

coupler (i.e. Port 1or Port 4 is the input port, and Port 2 and Port 3 are the output ports; the parameters given in the third column of Table 3.1 are used for the simulation).

From Fig 3.3 (a), when feeding from port 1(Σ port), it is observed that the return loss S_{11} and isolation S_{31} is higher than 20 dB; S_{21}=3.27 dB and S_{41}=2.97 dB at the design frequency (1 GHz). For the phase response (as shown in Fig. 3.3 (b)), the phase difference between the output ports is less than 5°. When feeding from port 3 (Δ port), the magnitudes of the *S*-parameters are shown in Fig 3.3 (c). The return loss $|S_{33}|$=23.5 dB while the isolation $|S_{13}|$=22.4 dB, and $|S_{23}|$=2.97 dB, $|S_{43}|$=3.1 dB. The phase difference between the output ports is almost 180 degree (as shown in Fig 3.3 (d)). All of these results have clearly proved that the designed coupler works as a rat-race coupler under this mode.

In Fig 3.4 (a), the magnitudes of the output signals are $|S_{21}|$=3 dB, $|S_{31}|$=3.5 dB. The isolation and the return loss are $|S_{41}|$=13 dB, $|S_{11}|$=27 dB. In Fig 3.4 (b), the phase difference between Port 2 and Port 3 is 87 degree. Therefore, it is proved that this structure can work as a 90-degree coupler with good isolation and matching performance.

In practice, by electronically controlling the capacitance values of varactors within the proposed coupler following Table 3.1, its performance can be reconfigured from a 90-degree coupler to a rat-race coupler and vice versa.

3.3 Conclusions

In this chapter, a novel reconfigurable directional coupler with a symmetrical structure has been presented. The designed coupler can be reconfigured from a 90-

degree coupler to a rat-race coupler (for the first time in this field). Based on the even-odd mode method, the analytical design equations for the proposed structure are derived. Furthermore, numerical simulation of the proposed coupler is conducted. The results match well with the design theory. During the reconfiguration, low return loss and high isolation are maintained, indicating good performance of proposed reconfigurable coupler.

CHAPTER 4

DESIGN OF MICROWAVE BALUNS WITH GENERALIZED STRUCTURES

4.1 Introduction

Balun (balanced-to-unbalanced) is a kind of widely used microwave devices that can find applications in microwave circuits/systems such as antenna feeding networks [29]-[31], amplifiers [32]-[35], and mixers [36]-[38]. In general, when an unbalanced signal is applied to the balun's input port, it will be transformed to balanced signals which have a 180-degree phase difference at the balun's output ports and vice versa [30]. Recently, more design requirements such as reduced size [39]-[45], good adaptability to different systems, and simplified shape for the baluns are imposed with the rapid development of the modern communication technology.

In the past, for the transmission-line-based baluns, the length of each branch within the balun is normally fixed to be λ/2 or λ/4 [46], [47] Due to this fact, the size of the balun is normally not compact, and the structure of it is not very flexible for practical applications. To address these issues, several different structures of baluns had been studied in the past. In [46], [47], the authors introduced different ways of designing new types of baluns with various characteristics. However, lumped components are employed in these structures. This may make the performance of the balun to be degraded at higher frequency bands. Moreover, with the introduction of the lumped components, the structure will be hard to be constructed and integrated, and even the cost will be higher. Therefore, new structures of transmission-line-based baluns are highly desired. Also, some existing balun structures do not use lumped components.

However, these baluns normally have very complex structures (e.g. too many tapped stubs), which makes them not practical for real implementations.

In this chapter, a symmetric balun structure is introduced based on a four-port network with the fourth port open-circuited. Two different types of baluns are designed using this structure. Explicit design equations are derived for both baluns. It is observed that transmission lines with arbitrary electrical lengths can be applied to the new baluns. Therefore, this balun has a high flexibility for practical implementations. In the proposed Type-I balun, a symmetric network equivalent to a λ/4 impedance transformer is employed. The corresponding design equations are derived using the ABCD matrix [48]. For the Type-II balun, an asymmetric impedance transforming network is applied, which will lead to further size reductions of proposed baluns.

To prove the design theory, the performance of proposed baluns is simulated, demonstrating the desired balun operation. Furthermore, an experimental prototype of these baluns is designed, fabricated and characterized. The measurement results match well with the simulation and theoretical results, validating the proposed design theory.

This chapter is organized as the following: In Section 4.1, a general introduction of the balun structure and the two designs is presented. In Section 4.2, general design principle of proposed generalized baluns and theoretical analysis of the first type of proposed baluns are discussed. In Section 4.3, theoretical analysis of the second type of generalized baluns is presented. Sections 4.4 and 4.5 show the simulation and measurement results of proposed baluns. Section 4.6 concludes this chapter.

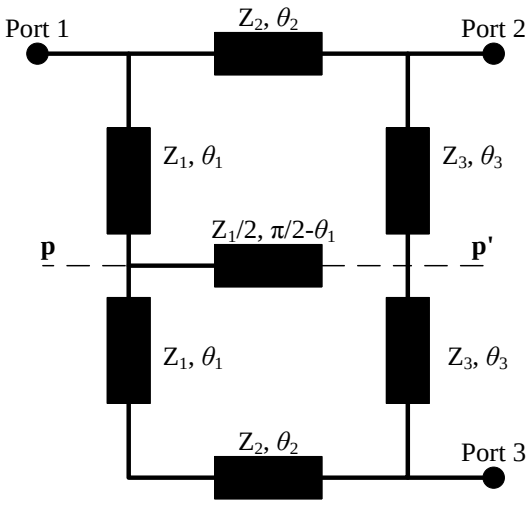

Fig. 4.1. The schematic of the proposed generalized baluns.

4.2 General Operating Principle of Proposed Generalized Baluns and Theoretical Analysis of the First Type of Proposed Baluns (Type-I)

The general schematic of the proposed baluns is shown in Fig. 4.1. It is composed of four different transmission lines. Three of them (with impedances of Z_1, Z_2, Z_3 as shown in Fig. 4.1) form the outer frame of the balun. The electrical lengths of these transmission lines are θ_1, θ_2, and θ_3, respectively. A shunted stub (with an impedance of $Z_1/2$) is attached to the center of the left branch (as shown in Fig. 4.1) and its electrical length is $\pi/2 - \theta_1$. As mentioned earlier, this device can be treated as a four-port network with its fourth port set to be open-circuited. The performance of this device can be analyzed using the even-odd mode method [48]. Assuming PP' as shown in Fig. 4.1 is the symmetric plane, the corresponding equivalent circuits under the even- and odd-mode excitations are illustrated in Fig. 4.2 (a) and (b).

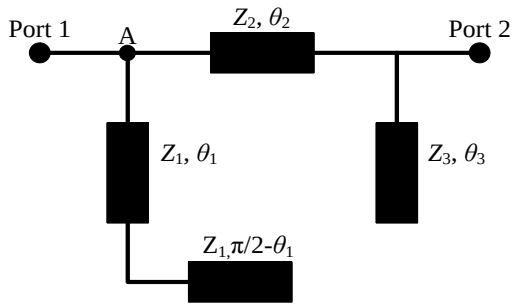

(a)

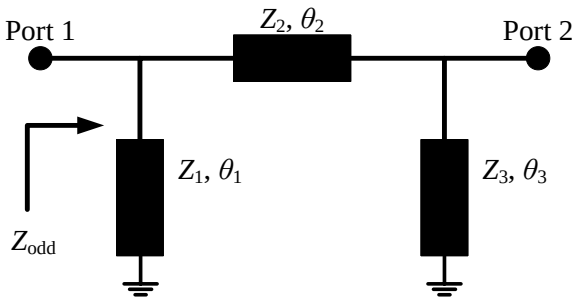

(b)

Fig. 4.2. Equivalent circuit models of the proposed device under (a) Even-mode excitation. (b) Odd-mode excitation.

In principle, in order to achieve the balun operation, the following conditions need to be satisfied [46], [47]:

$$T_{even} = 0 \tag{4-1}$$

$$Z_{odd} = 2Z_0 \tag{4-2}$$

where Z_0 is equal to 50 Ω (system impedance in most of microwave systems), T_{even} is the transmission coefficient under the even-mode excitation, and Z_{odd} is as labeled in Fig. 4.2(b).

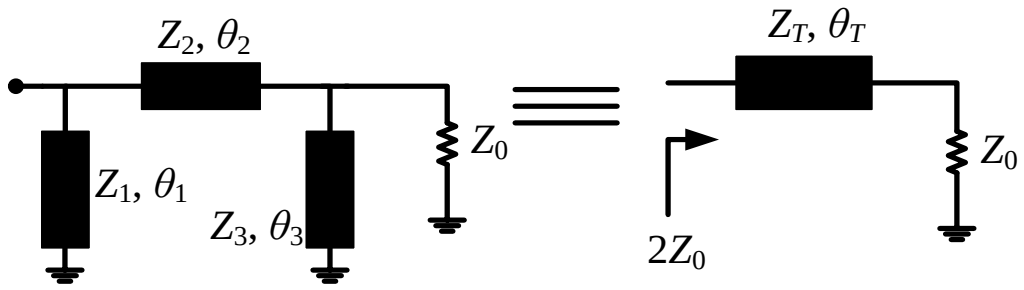

Fig. 4.3. The equivalent circuit of the λ/4 impedance transformer and the odd-mode circuit of the balun.

In the proposed two types of baluns, the even-mode condition (4-1) is realized based on the same working mechanism, which will be explained as follows. As shown in Fig. 4.2(a), under the even-mode excitation, the shunted stub (Z_1/2, π/2- θ_1) and the first transmission line (Z_1, θ_1) can be treated as a whole part which has the characteristic impedance of Z_1, and an electrical length of π/2. Therefore, they jointly form a shunted quarter-wavelength open-ended transmission line. As a result, point A (as marked in Fig. 4.2(a)) is shorted to ground. Under this condition, there is no signal can be transmitted from port 1 to port 2. In this way, (4-1) (i.e. $T_{even} = 0$) is always satisfied at the design frequency no matter which characteristic impedances and electrical lengths are given to the other two transmission lines (Z_2, and Z_3). Also, the impedance of Z_1 can be arbitrarily chosen as long as the characteristic impedance of the shunted stub is Z_1/2 and the total electrical length of these two sections is π/2.

Next, to satisfy (4-2) under the odd-mode excitation, different circuit topologies are employed, leading to the proposed Type-I and Type-II generalized baluns. First, the Type-I design is discussed. In this design, the odd-mode equivalent circuit (as shown in Fig. 4.2 (b)) is treated as a whole, which behaves as a transmission line with an

impedance of Z_T and an electrical length of θ_T (as shown in Fig. 4.3). To satisfy (4-2), the following relation needs to be satisfied:

$$2Z_0 = Z_T \frac{Z_0 + jZ_T \tan\theta_T}{Z_T + jZ_0 \tan\theta_T} \tag{4-3}$$

A straightforward solution to (4-3) will be $\theta_T = \pi/2$ and $Z_T = \sqrt{2}\,Z_0$, which corresponds to a λ/4 impedance transformer. To reach this condition, in the proposed Type-I design, the ABCD matrix of circuit shown in the left of Fig. 4.3 needs to be equal to that of the structure shown in the right of Fig. 4.3.

The ABCD matrix of the circuit shown in the right of Fig. 4.3 is given in (4-4).

$$\begin{bmatrix} A_T & B_T \\ C_T & D_T \end{bmatrix} = \begin{bmatrix} \cos\theta_T & jZ_T \sin\theta_T \\ \dfrac{j\sin\theta_T}{Z_T} & \cos\theta_T \end{bmatrix} = \begin{bmatrix} 0 & j\sqrt{2}Z_0 \\ \dfrac{j}{\sqrt{2}Z_0} & 0 \end{bmatrix} \tag{4-4}$$

By defining $Z_{in1}=jZ_1\tan\theta_1$ and $Z_{in3}=jZ_3\tan\theta_3$, the ABCD matrix of the structure shown in the left of Fig. 4.3 (i.e. the odd-mode circuit of Type-I balun) can be deduced as (4-5).

$$\begin{bmatrix} A_{odd} & B_{odd} \\ C_{odd} & D_{odd} \end{bmatrix} = \begin{bmatrix} 1 & 0 \\ \dfrac{1}{Z_{in1}} & 1 \end{bmatrix} \begin{bmatrix} \cos\theta_2 & jZ_2 \sin\theta_2 \\ \dfrac{j\sin\theta_2}{Z_2} & \cos\theta_2 \end{bmatrix} \begin{bmatrix} 1 & 0 \\ \dfrac{1}{Z_{in3}} & 1 \end{bmatrix}$$

$$= \begin{bmatrix} \cos\theta_2 + \dfrac{Z_2 \sin\theta_2}{Z_3 t_3} & jZ_2 \sin\theta_2 \\ \dfrac{j\cos\theta_2}{Z_1 t_1} + \dfrac{j\sin\theta_2}{Z_2} - \dfrac{jZ_2 \sin\theta_2}{Z_1 t_1 Z_3 t_3} - \dfrac{j\cos\theta_2}{Z_3 t_3} & \dfrac{Z_2 \sin\theta_2}{Z_1 t_1} + \cos\theta_2 \end{bmatrix} \tag{4-5}$$

where t_1, t_2, t_3 in (4-5) represent $\tan\theta_1$, $\tan\theta_2$, $\tan\theta_3$, respectively.

By equating D_T to D_{odd} and A_T *to* A_{odd} in (4-4) and (4-5), Z_1t_1 and Z_3t_3 should be the same value. In the proposed Type-I design, we have assumed that $Z_1 = Z_3 = Z$, and $t_1 = t_3 = t$ ($t = \tan\theta$). Therefore, it features a symmetrical impedance transformation network. Following this condition, the following equation is derived:

$$\cos\theta_2 = -\frac{Z_2 \sin\theta_2}{Zt} \tag{4-6}$$

Substituting (4-6) to the equations $C_{odd}=C_T$ and $B_{odd}=B_T$, (4-7) is derived:

$$Z_2 \sin\theta_2 = \sqrt{2}Z_0 \tag{4-7}$$

Equations (4-6) and (4-7) are the two key design equations of proposed Type-I generalized balun, from which all the parameters of the balun can be determined. Since there are multiple variables in (4-6) and (4-7) (i.e. Z_2, Z, θ_2, θ), the solutions of them are not unique, leading to flexible implementations. Two typical solutions of the Type-I balun are listed in Table 4.1. Meanwhile it is noted from (4-6), because the characteristic impedance Z_2, and Z are positive values, if t ($\tan\theta$) is positive, $\tan\theta_2$ must be negative and vice versa. This means in the practical realization, the electrical length of one of these two transmission lines (θ_2 and θ) must be larger than 90 degree. If a more compact design is needed, and a fully symmetric structure is not required, the Type-II design is proposed. More details of it are discussed in the next section.

TABLE 4.1
Calculated Design Parameters of Type-I Balun

	Solution 1	Solution 2
$Z_2(\Omega)$	100	81.65
θ_2(degree)	135	120
$Z(\Omega)$	100	81.65
$\theta = \theta_1 = \theta_3$ (degree)	60	60

4.3 Theoretical Analysis of the Second Type of Proposed Generalized Baluns (Type-II)

In the previous section, it is shown that a symmetric network (with $Z_1 = Z_3$, $\theta_1 = \theta_3$) which is equivalent to a quarter-wavelength impedance transformer can be used to satisfy (4-2), leading to the proposed Type-I balun. Here in this section, by breaking the symmetry (i.e. $Z_1 \neq Z_3$, $\theta_1 \neq \theta_3$), it will be shown that (4-2) can also be satisfied. The resulting structure is the Type-II balun. The design equations for this type of baluns are derived as follows.

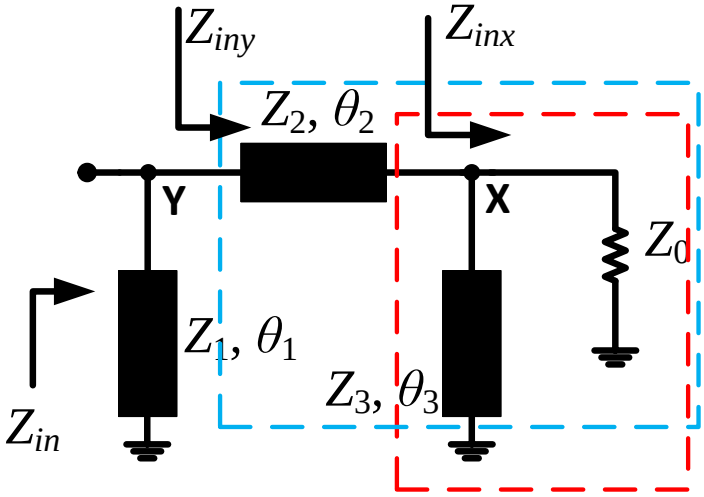

Fig. 4.4. The input impedance of the equivalent circuit under odd-mode excitation for the Type-II balun.

Referring to Fig. 4.4, the input impedance looking into Port 1 is defined as Z_{in}, and the impedance looking into Node X and Node Y are represented by Z_{inx} and Z_{iny}, respectively. In order to meet (4-2), the following equations are derived.

$$Z_{inx} = \frac{1}{\frac{1}{Z_0} + \frac{1}{jZ_3 t_3}} \tag{4-8}$$

$$Z_{iny} = \frac{Z_2 Z_{inx} + jZ_2^2 t_2}{Z_2 + jZ_{inx} t_2} \tag{4-9}$$

$$Z_{in} = \frac{1}{\frac{1}{jZ_1 t_1} + \frac{1}{Z_{iny}}} = 2Z_0 \tag{4-10}$$

Again Z_0 is equal to 50 Ω. And Z_{in} is assumed to be 100 Ω in this paper. Therefore, to satisfy (4-10) (equivalent to (4-2)), its real part should be equal to 100 while its imaginary part should be equal to 0.

$$\mathrm{Re}[Z_{odd}] = 2Z_0 = 100 \tag{4-11}$$

$$\mathrm{Im}[Z_{odd}] = 0 \tag{4-12}$$

Equations (4-10)-(4-12) are the key design equations for the Type-II generalized balun. Again, the solutions of these equations are not unique. By numerically solving these equations using Matlab and assuming all electrical lengths are less than 90° (for the purpose of compactness), different sets of solutions can be found. Some of them

are listed in Table 4.2. As desired, the Type-II design also features flexible implementations. Overall, the proposed Type-I and Type-II baluns represent a generalized balun structure.

TABLE 4.2
Calculated Design Parameters of Type-II Balun

	Solution 1	Solution 2	Solution 3
$Z_1(\Omega)$	52	35.5	46
θ_1(degree)	60	45	60
$Z_2(\Omega)$	15	15.5	35
θ_2(degree)	56	74	79
$Z_3(\Omega)$	15	13	32.7
θ_3(degree)	45	45	45

4.4 Simulation Results

To verify the design theories, the proposed two types of baluns are simulated in HyperLynx (previously called IE3D). In the Type-I design, the working frequency of the balun is 2.4GHz. The key design parameters of the balun are listed in Table 4.1 (Solution 2). The magnitude and the phase of the *S*-parameters of this balun are shown in Fig. 4.5 and Fig. 4.6. From these two figures, the characteristics of this balun can be summarized as the following:

- The return loss ($|S_{11}|$) is very low (much lower than -50 dB) at 2.4 GHz, which means good matching at the input port (Port 1).
- At the working frequency 2.4 GHz, the magnitude of S_{21} and S_{31} are equal, which is 3 dB. This indicates the power is equally split into the two output ports (Port 2 and Port 3).
- The phase difference between the two output ports is 180 degree at the design

frequency.

- The bandwidth of this balun is wide (almost 300 MHz).

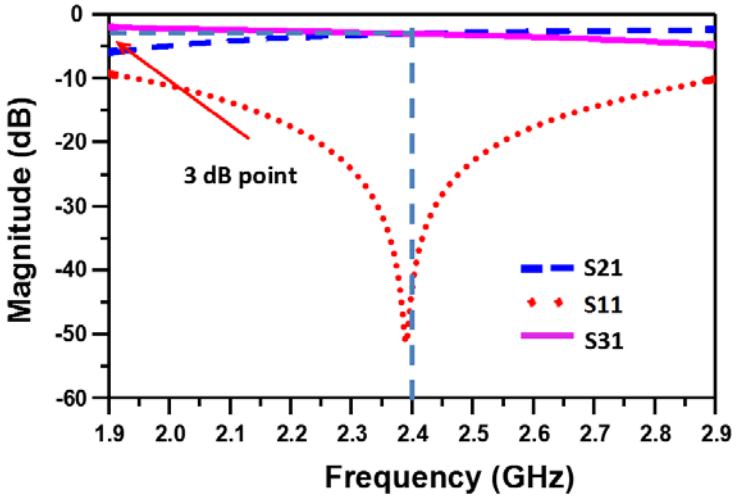

Fig. 4.5. The magnitude of the simulated *S*-parameters of the Type-I design.

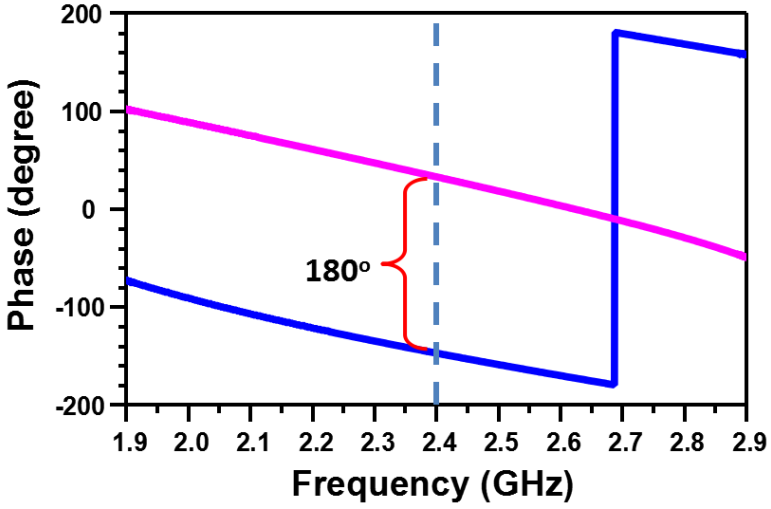

Fig. 4.6. The phase of the simulated *S*-parameters of the Type-I design.

It is clear that the simulated results match well with the theoretical analysis.

For the Type-II design, a compact balun is designed, which again works at 2.4 GHz. The key design parameters of this balun are listed in Table 4.2 (Solution 3). The simulated magnitude and phase responses of this balun are shown in Fig. 4.7 and Fig. 4.8. From Fig. 4.7, it is observed that at the working frequency, the magnitude of S_{21} and S_{31} are also equal to 3 dB, and $|S_{11}|$ is as low as 25 dB. Furthermore, in Fig. 4.8, the phase difference between the two output signals is 180 degree.

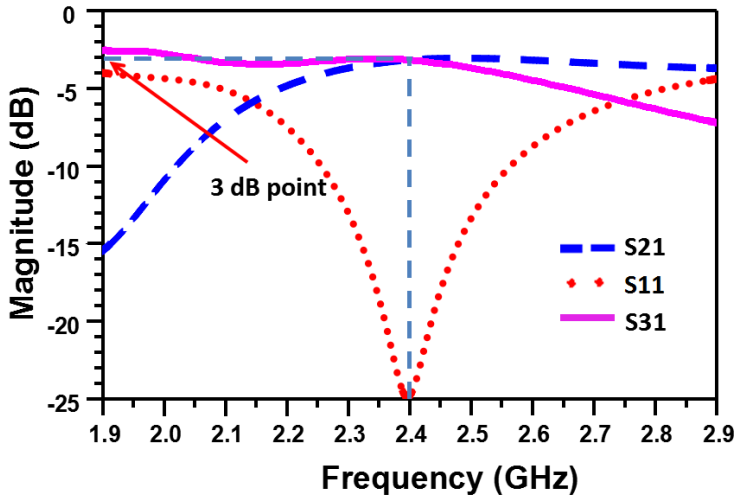

Fig. 4.7. The magnitude of the simulated *S*-parameters of the Type-II design.

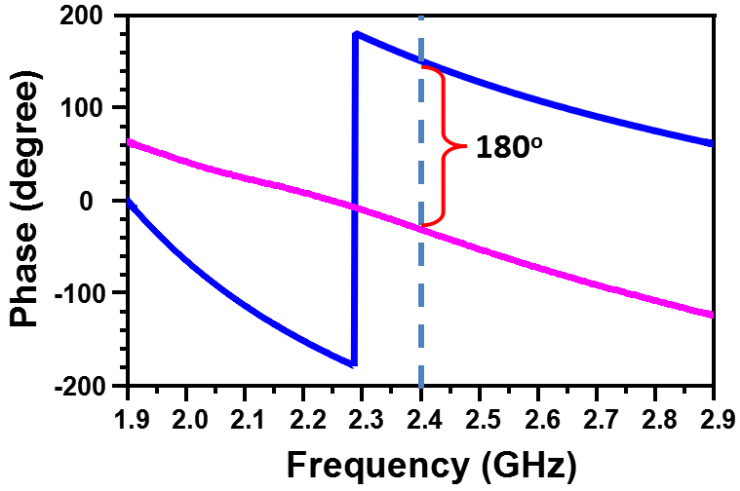

Fig. 4.8. The phase of the simulated *S*-parameters of the Type-II design.

4.5 Fabrication and Measured Results

In order to validate the performance of proposed generalized baluns, one of the prototypes designed in the previous section is fabricated. This device is built on the RT/Duriod 5880LZ printed circuit board. The substrate thickness is 0.762 mm, the dielectric constant is 1.96, and the loss tangent is 0.0019.

Fig. 4.9 shows the photo of the device. The balun is designed by the Type-I method. Again, the key dimensions of it are listed in Table 4.1 (Solution 2). As shown in Fig. 4.9, the characteristic impedance Z_1 is equal to Z_3 and they are represented by Z in this figure. The electrical length θ_1 is equal to θ_3 and they are represented by θ. In the experimental prototype, Z = 81.65 Ω and θ = 60° are applied. Also, the open-circuited Port 4 is marked in this figure.

The measured magnitudes of S_{11}, S_{21}, and S_{31} are shown in Fig. 4.10. Fig. 4.11 shows the measured phase responses at the two output ports (Port2 and Port 3).

From these two figures, the characteristics of the designed balun can be summarized as the following:

- Comparing the simulation and measurement results, a small phase shift of around 10 MHz is observed, which is due to the fabrication tolerance.
- At the working frequency, the return loss (S_{11}) is very good (47 dB).
- The magnitudes of the output signals are almost equal to each other. Both of them are close to 3 dB (e.g. $|S_{21}|$ = 3.11 dB, and $|S_{31}|$ = 2.97 dB at the center frequency).
- The phase difference between the two output signals is very close to 180° (181° in the measured data).

- The bandwidth of the experimental prototype is larger than 200 MHz.

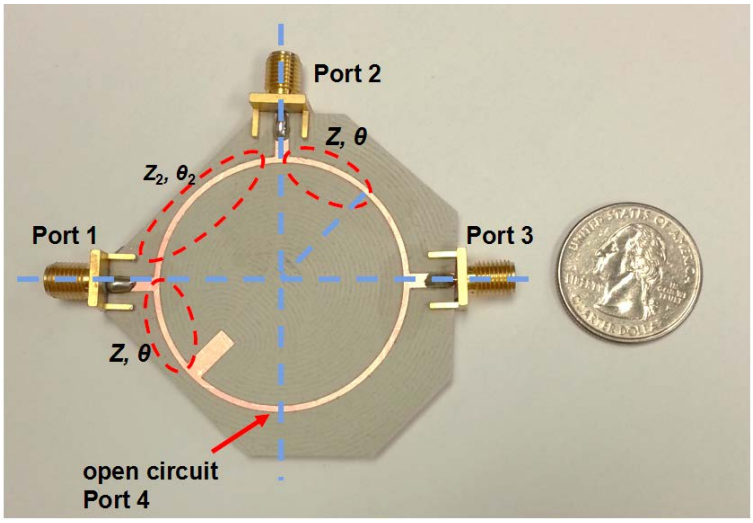

Fig. 4.9. The photo of the fabricated prototype.

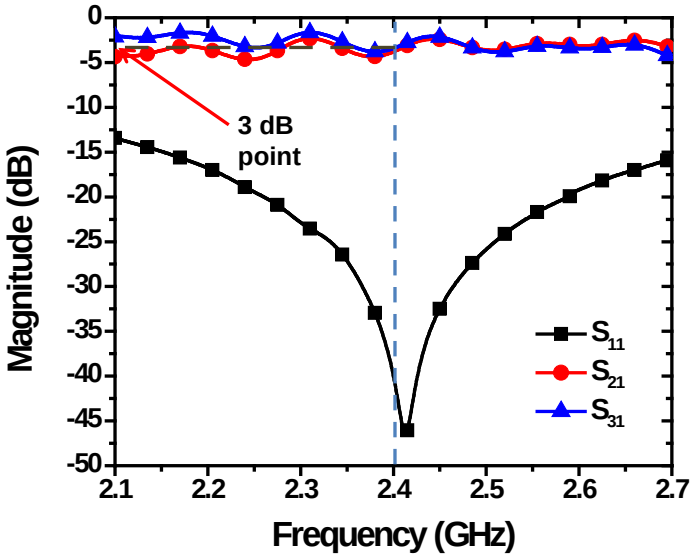

Fig. 4.10. The measured magnitude of the *S*-parameters of the device.

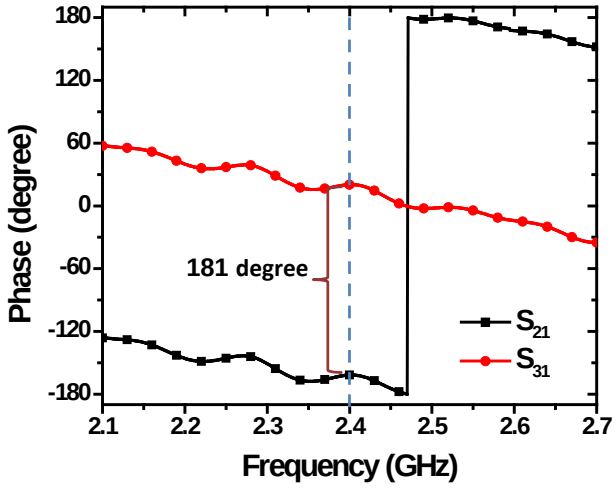

Fig. 4.11. The measured phase responses of S_{21} and S_{31}.

Overall, the measured results are in good agreement with the simulation results as well as the theoretical analysis. It clearly verifies the design theory of proposed generalized baluns.

4.6 Conclusion

In this chapter, two different ways of designing generalized microwave baluns are presented. The proposed baluns are designed based on a symmetric four-port network with the fourth port open-circuited. Specifically, symmetric and asymmetric impedance transforming networks are employed in proposed baluns, leading to Type-I and Type-II baluns. Applying the even-odd mode method, explicit design equations are derived for both designs. The proposed design theory is validated by simulation and measurement results. In general, the proposed two types of baluns represent a generalized implementation of microwave baluns, which is flexible for practical realization. They can also offer attractive characteristics such as wide bandwidth and compact size.

CHAPTER 5

CONCLUSION AND FUTURE WORK

In this thesis, several new designs of tunable/reconfigurable and compact microwave devices were introduced. For all these devices discussed in previous chapters, rigorous theoretical analysis and design equations of them were presented. After the theoretical analysis, these components were implemented and tested. First, a tunable coupler was designed. This coupler has a fully symmetrical structure. Its power splitting ration can be tuned easily by changing the capacitance loaded at the symmetric plane while the phase difference is kept as 90 degree. Furthermore, when the capacitance is tuned to be 0 or a very small value, this device can be reconfigured to be a crossover. Then, a reconfigurable coupler was introduced. Closed form equations were derived to verify the design theory. Moreover, a device was built and simulated. The tested results under two operating states were shown to match with the simulated and theoretical results. Good agreement was achieved. Finally, two types of generalized balun structures were discussed. By using the proposed structures, the branches of the balun can have an arbitrary electrical length, which can lead to a compact size. Also, one of the proposed baluns was fabricated to verify the design theory.

In the future, in order to further improve the performance of the tunable/reconfigurable and the generalized compact microwave devices, more different designs with new structures need to be investigated. Furthermore, the theories of the proposed devices need to be further studied. In general, tunable and compact devices have a great potential in the real applications. The systems based on this kind of

devices will have compact size and good adaptability to different specifications.

REFERENCES

[1] D. M. Pozar, Microwave Engineering, 4th ed. NJ:WILEY, 2011.

[2] B. R. Heimer, L. Fan, and K. Chang, “Uniplanar hybrid couplers using asymmetrical coplanar striplines,” IEEE Trans. Microw. Theory Tech., vol. 45. no. 12, pp. 2234-2240, Dec. 1997.

[3] K. Chin, M. Ma, Y, Chen, Y, Chiang, “Closed-form equations of conventional microstrip couplers applied to design couplers and filters constructed with floating-plate overlay,” IEEE Trans. Microw. Theory Tech., vol. 56. no. 5, pp. 1172-1179, May. 2008.

[4] M. A. Y. Abdalla, K. Phang, and G. V. Eleftheriades, “A compact highly reconfigurable COMS MMIC directional coupler,” IEEE Trans. Microw. Theory Tech., vol. 56. no. 2, pp. 305-319, Feb. 2008.

[5] K. Cheng and F. Wong, “A novel approach to the design and implementation of dual-band compact planar 90° branch-line coupler,” IEEE Trans. Microw. Theory Tech., vol. 52, no. 11, pp. 2458-2463, Nov. 2004.

[6] K. M. Cheng and S. Yeung, “A novel rat-race coupler with tunable power dividing ratio, ideal port isolation, and return loss performance,” IEEE Trans. Microw. Theory Tech., vol. 61, no. 1, pp. 55-60, Jan. 2013.

[7] J. J. Yao, C. Lee, and S. P. Yeo, “Microstrip branch-line couplers for crossover application,” IEEE Trans. Microw. Theory Tech., vol. 59, no. 1, pp. 87-92, Jan. 2011.

[8] X. Wang, W. Yin, and K. Wu, “A dual- band coupled-line coupler with an arbitrary coupling coefficient,” IEEE Trans. Microw. Theory Tech., vol. 60, no. 4, pp. 945-951, Apr. 2012.

[9] J. Shao, H. Ren, B. Arigong, C. Li, and H. Zhang, “A fully symmetrical crossover and its dual-frequency application,” IEEE Trans. Microw. Theory Tech., vol. 60, no. 8, pp. 2410-2416, Aug. 2012.

[10] F. Wong and K. M. Cheng, “A novel, planar, and compact crossover design for dual-band applications,” IEEE Trans. Microw. Theory Tech., vol. 59, no. 3, pp. 568-573, Mar. 2011.

[11] J. Shao, H. Zhang, Y. Lin, and H. Xin, “Dual-frequency electromagnetic cloaks enabled by LC-based metamaterial circuits,” Progr. Electromagn. Res. C, vol. 22, pp. 109-122, 2011.

[12] E. E. Djoumessi, E. Marsan, C. Caloz, M. Chaker, and K. Wu, “Varactor-tuned dual-band quadrature hybrid coupler,” IEEE Microw. Wireless Compon. Lett., vol. 16, no.11, pp. 603-605, Nov. 2006.

[13] S. Lee, and Y. Lee, “Wideband branch-Line coupler with single section quarter-wave transformers for arbitrary coupling levels,” IEEE Microw. Wireless Compon. Lett., vol. 16, no. 11, pp. 603-605, Nov. 2006.

[14] L. Chiu, and Q. Xue, “Investigation of a wideband 90° hybrid coupler with an arbitrary coupling level,” IEEE Trans. Microw. Theory Tech., vol. 58, no. 4, pp. 1022-1029, Apr. 2010.

[15] W. A. Arriola, J. Y. Lee, and I. S. Kim, “Wideband 3 dB branch line coupler based on λ/4 open circuited coupled lines,” IEEE Microw. Wireless Compon. Lett., vol. 21, no. 9, pp. 486-488, Sep. 2011.

[16] A. M. Abbosh, and, M. E. Bialkowski, “Design of compact directional couplers for UWB applications,” IEEE Trans. Microw. Theory Tech., vol. 55, no. 2, Feb. 2007.

[17] C. S. Kim, C. S. Yoon, J. Park, D. Ahn, J. Lim, and S. Yang, “A design of the novel varactor tuned directional coupler,” in IEEE MTT-S Int. Microw. Sump. Dig., Jun. 1999, vol. 4, pp. 1725-1728.

[18] C. S. Kim, J. S. Park, D. Ahn, and J. B. Lim, “Variable directional coupler with LC resonator,” Electron. Lett., vol. 36, no. 18, pp. 1557-1559, Aug. 2000.

[19] E. A. Fardin, K. Ghorbani, and A. S. Holland, “A varactor tuned branch-line hybrid coupler,” in Proc. Asia-Pacific Microw. Conf., Dec. 2005, vol. 3, pp. 4-7.

[20] E. A. Fardin, A. S. Holland, and K. Ghorbani, “Electronically tunable lumped element 90° hybrid coupler,” Electron. Lett., vol. 42, no. 6, pp. 353-355, Mar. 2006.

[21] H.H. Hsieh, Y. Liao, and L. Lu, “A compact quadrature hybrid MMIC using CMOS active inductors,” IEEE Trans. Microw. Theory Tech., vol. 55, no. 6, pp. 1098-1104, Jun. 2007.

[22] K. Shibata, K. Hatori, Y. Tokumitsu, and H. Komizo, “Microstrip spiral directional coupler,” IEEE Trans. Microw. Theory Tech., vol. 29, no. 7, pp. 680-689, Jul. 1981.

[23] J. Sun, C. Li, Y. Geng, and P. Wang, “A highly reconfigurable low-power CMOS directional coupler,” IEEE Trans. Microw. Theory Tech., vol. 60, no. 9, pp. 2815-2822, Sep. 2012.

[24] R. E. Collin, Foundations for Microwave Engineering, 2nd ed. New York: McGraw-Hill, 1992.

[25] Data Sheet-SMV1265 Series Hyperabrupt Junction Tuning Varactors, Skyworks Solutions Inc, Woburn, MA, 2011.

[26] M. Zhou, J. Shao, B. Arigong, H. Ren, R. Zhou, and H. Zhang, “A Varactor Based 90◦ Directional Coupler With Tunable Coupling Ratios and Reconfigurable Responses,” IEEE Trans. Microwave Theory & Tech., accepted in Jan. 2014 (early access).

[27] C. A. Balanis, Antenna Theory, 3rd ed. NJ:WILEY, 2005.

[28] W. Wang, T. Shen, T .Huang, and R. Wu, “Miniaturized Rat-Race Coupler with Bandpass Response and Good Stopband Rejection,” International Microwave Symposium Digest, Boston, MA, 2009, pp. 709-712.

[29] H. Zhang, H. Xin, “A Dual-Band Dipole Antenna With Integrated-Balun,” IEEE Trans. Antennas and Propagation, vol. 57. no. 3, pp. 786-789, 2009.

[30] C. A. Balanis, Antenna Theory, Analysis and Design, 1st ed. New York: Wiley, 1982.

[31] E. W. Reid, L. Ortiz-Balbuena, and K. Moez, “Integrated Low-Loss Balun for Vivaldi Antennas,” Electron. Lett., vol. 49, no. 9, pp. 442-444, April 2009.

[32] G. Engargiola, “Tapered Microstrip Balun for Integrating A Low Noise Amplifier with A Nonplanar Log Periodic Antenna,” Review of Scientific Instruments, vol. 74. no. 12, pp. 5197-2500, 2003

[33] A. Jahanian, P. Heydari, “A CMOS Distributed Amplifier with Distributed Active Input Balun Using GBW and Linearity Enhancing Techniques,” IEEE Trans. Microw. Theory Tech., vol. 60. no. 5, pp. 1331-1341, May 2012.

[34] V. A. Solomko, and P. Weger, “A Fully Integrated 3.3-3.8-GHz Power Amplifier with Autotransformer Balun,” IEEE Trans. Microw. Theory Tech., vol. 7. no. 9, pp. 2160-2172, September 2009.

[35] Y. Ji, C. Wang, J. Liu, and H. Liao, “1.8 dB NF 3.6 mW CMOS Active Balun Low Noise Amplifier for GPS,” Electron. Lett., vol. 46, no. 3, pp. 251-252, February 2010.

[36] H Chiou, and T. Yang, “Low-Loss and Broadband Asymmetric Broadside-Coupled Balun for Mixer Design in 0.18-um CMOS Technology,” IEEE Trans. Microw. Theory Tech., vol. 56, no. 4, pp. 835-848, April 2008.

[37] C. Kim, H. Son, B. Kang, “A 2.4 GHz Current-Reused CMOS Balun-Mixer,” IEEE Microw. Wireless Compon. Lett., vol. 19, no. 7, pp. 464-466, July 2009.

[38] P. Yeh, W. Liu, and H. Chiou, “Compact 28 GHz Subharmonically Pumped Resistive Mixer MMIC Using a Lumped-Element High-Pass/Band-Pass Balun,” IEEE Microw. Wireless Compon. Lett., vol. 15, no. 2, pp. 62-64, February 2005.

[39] H. Ahn, T. Itoh, “New Isolation Circuits of Compact Impedance-Transforming 3-dB Baluns for Theoretically Perfect Isolation and Matching,” IEEE Trans. Microw. Theory Tech., vol. 58, no. 12, pp. 3892-3902, December 2010.

[40] X. Miao, W. Zhang, Y. Geng, X. Chen, R. Ma, J. Gao, “Design of Compact Frequency-Tuned Microstrip Balun,” IEEE Antennas and Wireless Propagation Letters, vol. 9, pp. 686-688, 2010.

[41] B. P. Kumar, and G. R. Branner, “Optimized Design of Unique Miniaturized Planar Baluns for Wireless Applications,” IEEE Microw. Wireless Compon. Lett., vol. 13, no. 2, pp. 134-136, February 2003.

[42] K. Nishikawa, I. Toyoda, and T. Tokumitsu, “Compact and Broad-band Three-dimensional MMIC Balun,” IEEE Trans. Microw. Theory Tech, vol. 47, no.1, pp. 96-98, January 1999.

[43] C. Shie, Y. Pan, K. Chin, and Y. Chiang, “A Miniaturized Microstrip Balun Constructed with Two λ/8 Coupled Lines and a Redundant Line,” IEEE Microw. Wireless Compon. Lett., vol. 20, no. 12, pp. 663-665, December 2010.

[44] C. Tsai, I. Ieong, H. Chen, and T. Wu, “A Miniaturized and Broadband Balun Using Artificial Coupled Line With Imaginary Even-Mode Impedance,” IEEE Trans. Microw. Theory Tech, vol. 59, no.9, pp. 2233-2240, September 2011.

[45] Y. Guo, Z. Y. Zhang, L. C. Ong, and M. Y. W. Chia, “A Novel LTCC Miniaturized Dualband Balun,” IEEE Microw. Wireless Compon. Lett., vol. 16, no. 3, pp. 143-145, March 2006.

[46] X. Gao, L. Yeung, K. Wu, “A Dual-Band Balun Using Partially Coupled Stepped-Impedance Coupled-Line Resonators,” IEEE Trans. Microw. Theory Tech, vol. 56, no.6, pp. 1455-1460, June 2008.

[47] K. Ang, Y. Leong, and C. Lee, “Analysis and Design of Miniaturized Lumped-Distributed Impedance-Transforming Baluns,” IEEE Trans. Microw. Theory Tech, vol. 51, no.3, pp. 1009-1017, March 2003.

[48] D. M. Pozar, Microwave Engineering, 4th ed. NJ: WILEY, 2011.